

SCIENTIFIC REPORTS



OPEN

Chromium removal from aqueous solution by a PEI-silica nanocomposite

Keunsu Choi¹, Soonjae Lee², Jin Ock Park³, Jeong-Ann Park⁴, So-Hye Cho^{3,5}, SeungYong Lee^{3,5}, Jun Hee Lee¹ & Jae-Woo Choi^{4,6}

It is essential and important to determine the adsorption mechanism as well as removal efficiency when using an adsorption technique to remove toxic heavy metals from wastewater. In this research, the removal efficiency and mechanism of chromium removal by a silica-based nanoparticle were investigated. A PEI-silica nanoparticle was synthesized by a one-pot technique and exhibited uniformly well-dispersed PEI polymers in silica particles. The adsorption capacity of chromium ions was determined by a batch adsorption test, with the PEI-silica nanoparticle having a value of 183.7 mg/g and monolayer sorption. Adsorption of chromium ions was affected by the solution pH and altered the nanoparticle surface chemically. First principles calculations of the adsorption energies for the relevant adsorption configurations and XPS peaks of Cr and N showed that Cr(VI), $[\text{HCrO}_4]^-$ is reduced to two species, Cr(III), CrOH^{2+} and Cr^{3+} , by an amine group and that Cr(III) and Cr(VI) ions are adsorbed on different functional groups, oxidized N and NH_3^+ .

The term “heavy metals” refers to metals with specific gravities of approximately 4.0 or higher, which are distributed mostly in rock and soil. Heavy metals produced by smelting processes are used for various purposes, such as batteries, blood pressure gauges, thermometers, building blocks, and in the machinery industry^{1–4}. Ions of heavy metals discharged from a wide range of industrial processes from anthropogenic sources have become serious environmental and human health problems^{4,5}.

Among the heavy metals, chromium is used in various industrial fields, such as the metallurgical, steel, tannery and cement industries, which are also major emission sources⁶. Chromium discharged from industries is most commonly in the form of trivalent (Cr(III)) or hexavalent (Cr(VI)) chromium in water⁷. Cr(III) is an essential human dietary element and, Cr(VI) occurs naturally in nature from the erosion of chromium deposits. These can also be produced by anthropogenic emissions, such as industrial processes. However, Cr(III) and Cr(VI) have significant differences related to their characteristics, including toxicological and biological properties⁶. Cr(VI) is considered to be a very harmful compound because of its characteristics of being water soluble and carcinogenic⁸. In contrast, Cr(III) is less soluble and relatively non-toxic over a wide pH range. Due to its toxicity, the US EPA and the EU established the permissible emission standards for Cr(III) and Cr(VI) as a total chromium amount of 0.1 mg/L in 1991⁶.

For these reasons, studies on reducing the amount of chromium below the effluent water quality standard are very important issues. Various techniques have been studied to purify chromium-contaminated water, including ion exchange^{9,10}, membrane processes¹¹, electrodialysis¹², precipitation¹³, bio-sorption¹⁴, photocatalytic degradation¹⁵, and adsorption^{16,17}. In addition, Cr(III) can be easily precipitated from the aqueous phase by hydroxide or

¹School of Energy and Chemical Engineering, Ulsan National Institute of Science and Technology, Ulsan, 44919, Republic of Korea. ²Department of Earth and Environmental Sciences, Korea University, 145, Anam-ro, Seongbuk-gu, Seoul, 02841, Republic of Korea. ³Materials Architecturing Research Center, Korea Institute of Science and Technology, Hwarang-ro 14-gil 5, Seongbuk-gu, Seoul, 02792, Republic of Korea. ⁴Center for Water Resource Cycle Research, Korea Institute of Science and Technology, Hwarang-ro 14-gil 5, Seongbuk-gu, Seoul, 02792, Republic of Korea. ⁵Division of Nano & Information Technology, KIST School, Korea University of Science and Technology, Hwarang-ro 14-gil 5, Seongbuk-gu, Seoul, 02792, Republic of Korea. ⁶Division of Energy & Environment Technology, KIST School, Korea University of Science and Technology, Hwarang-ro 14-gil 5, Seongbuk-gu, Seoul, 02792, Republic of Korea. Keunsu Choi, Soonjae Lee and Jin Ock Park contributed equally to this work. Correspondence and requests for materials should be addressed to S.Y.L. (email: patra@kist.re.kr) or J.H.L. (email: junhee@unist.ac.kr) or J.-W.C. (email: plead36@kist.re.kr)

oxide foams. Therefore, the chemical reduction of toxic Cr(VI) to Cr(III) by precipitation is a common method for the treatment of wastewater with Cr(VI)^{18,19}. However, unfortunately, this method increases the already huge production of sludge, resulting in limited field applications. Compared to other techniques, adsorption is the most promising technology due to its high efficiency, ease of operation, and economic advantages²⁰. Moreover, the greatest advantage of the adsorption method is that by-products, such as sludge, are not generated.

Various adsorbents for Cr(VI) removal, such as activated carbons, zeolites, clays, etc., have been investigated^{21–27}. However, silica is superior to the other materials mentioned above because of its high porosity, large surface area and great number of functionalities^{28,29}. For these reasons, a great amount of research on silica as Cr(VI) adsorbents has been carried out^{30–38}. Usually, the preparation of silica adsorbents consists of two stages, including the synthesis of porous silica and the attachment of functional groups for Cr(VI) adsorption onto the silica surface.

In this study, we investigated a PEI-silica nanoparticle, which was prepared by a simple one-step synthetic method, as an adsorbent to remove toxic chromium in solution. Furthermore, the adsorption capacity for chromium was extensively investigated, and its chromium adsorption mechanism was clarified, which may be applicable for silica-based materials in general.

Results and Discussion

Characteristics of the PEI-silica Nanoparticles. The electron microscopy analysis by SEM and TEM indicates that the particles have near spherical and elliptical morphologies (Fig. 1). The size of the particles is in the range of approximately 200–300 nm, as also shown in Fig. 1. The line scan result by TEM reveals that silicon and nitrogen atoms are uniformly distributed. This indicates that the PEI polymers are uniformly dispersed in the silica particles. Also, the TEM mapping result of nitrogen atoms supports the uniform dispersion of PEI polymers. (Fig. S1 in Supporting Information).

The surface areas and pore volumes of the silica nanoparticles were analyzed by the nitrogen (N_2) adsorption-desorption technique at 77 K. As shown in Fig. 2, the silica nanoparticles exhibited a characteristic type III BET isotherm graph, which indicates that the PEI-silica nanoparticles are essentially non-porous. This result agrees with the very small BET surface areas and pore volumes of the materials in Table 1. Therefore, amine groups exposed on the surface participate in the adsorption of Cr(VI).

In the FT-IR results, the strong absorption band at 1042 cm^{-1} is due to stretching asymmetric vibrations of the Si-O-Si band (Fig. 3)³⁹. The absorption peak at 787 cm^{-1} is assigned to the bending vibrations of Si-O-Si group, while the absorption peak at 609 cm^{-1} are ascribed to the symmetric stretching vibrations of the Si-O-Si band⁴⁰. It is thought that the absorption peak at approximately 961 cm^{-1} is related to the Si-O- groups. The existence of PEI is confirmed by the presence of absorption features of PEI at $1553\text{--}1646\text{ cm}^{-1}$. This peak is assigned to the bending of N-H₂^{41,42}. The two bands at 2853 cm^{-1} and 2923 cm^{-1} agree well with the C-H₂ absorption bands^{43,44}. The peak at 1468 is assigned to symmetric bending mode of NH₃³⁺ in the Si-O- ... NH₃³⁺ groups^{45,46}.

For further elemental analysis of the PEI-silica nanoparticles, an X-ray photoelectron spectroscopy (XPS) measurement was performed. The XPS spectrum of Si atoms in Fig. 4 consists of peaks with binding energies of 153 eV (Si 2s) and 103 eV (Si 2p)⁴⁶. Additionally, the C 1s and O 1s peaks in the PEI-silica nanoparticles were detected near 284 eV and 532 eV , respectively. The C 1s peak at approximately 285 eV typically corresponds to C-C and C-N bonds^{47,48}. As shown in Fig. 4(b), an asymmetric peak in the spectrum of C 1s consists of three peaks with binding energies of 284.58 , 285.87 and 288.11 eV . These are considered to originate from the conjunction bonding with adjacent N atoms by PEI⁴⁹. More importantly, the XPS spectrum in Fig. 4(c) at approximately 400 eV indicates the presence of N atoms with three different binding energies. The binding energies of N 1s are 398.66 , 399.66 and 402.09 eV . It is noticeable that the peak area portion of protonated amine groups, NH₃⁺, at 402.09 eV is only 11.7%, while most of the peak, 88.3%, originates from primary amines, secondary amines and their bonds with oxygens⁵⁰. It was reported that the content of primary amines, secondary amines, and tertiary amines of the PEI used in this research is 44%, 33%, 23%, respectively⁵¹. The content of PEI was evaluated by measuring the mass change after burning-out at 480°C for 12 hrs. The portion of PEI ranges from 37–40 wt%. Also, TG analysis showed similar PEI content, 42%. (Fig. S2 in Supporting Information).

Chromium Adsorption of the PEI-silica Nanoparticles. The applicability of the PEI-silica nanoparticles for the removal of Cr from aqueous solution was investigated by conducting equilibrium batch experiments. The reusability of PEI-silica was also validated through successive regeneration and reuse tests (Exp. S1 in Supplementary Information). Additionally, the effect of the solution pH on the chromium adsorption was investigated by adjusting the initial pH from 2 to 4. PEI-silica nanoparticles showed significant removal of chromium, but the pure nanosilica, in the control test, showed negligible chromium removal (data not shown) despite of a very large BET surface area, $1379.6\text{ m}^2\text{ g}^{-1}$. This indicated that the chromium removal resulted from the PEI group on the nanoparticle.

The chromium adsorption isotherms at the different pH levels are shown in Fig. 5. The PEI-silica nanoparticle exhibited non-linear and pH-dependent adsorption isotherms for the removal of chromium. The adsorption isotherms are well-fitted with the Langmuir adsorption model. The isotherms for pH values of 2, 3 and 4 exhibited high maximum adsorption capacities of 120.7, 138.2 and 183.7 mg/g, respectively. The isotherms of initial pH values of 2 and 3 showed similar rate of adsorption (similar K_a), but the isotherm of the pH of 4 showed a different trend than the others, with a much lower K_a . This shows that the chromium removal capacity of the PEI silica nanoparticle increased in the higher pH conditions, but the chromium adsorption reaction was different at higher pH conditions. The chromium adsorption capacity of PEI-silica nanoparticles was higher than those presented in previous research related to chromium removal using adsorbents, including surface-functionalized mesoporous iron oxyhydroxide (25.05 mg/g), magnetite (4.84 mg/g), nanocarbon (27.29 mg/g), coconut-derived

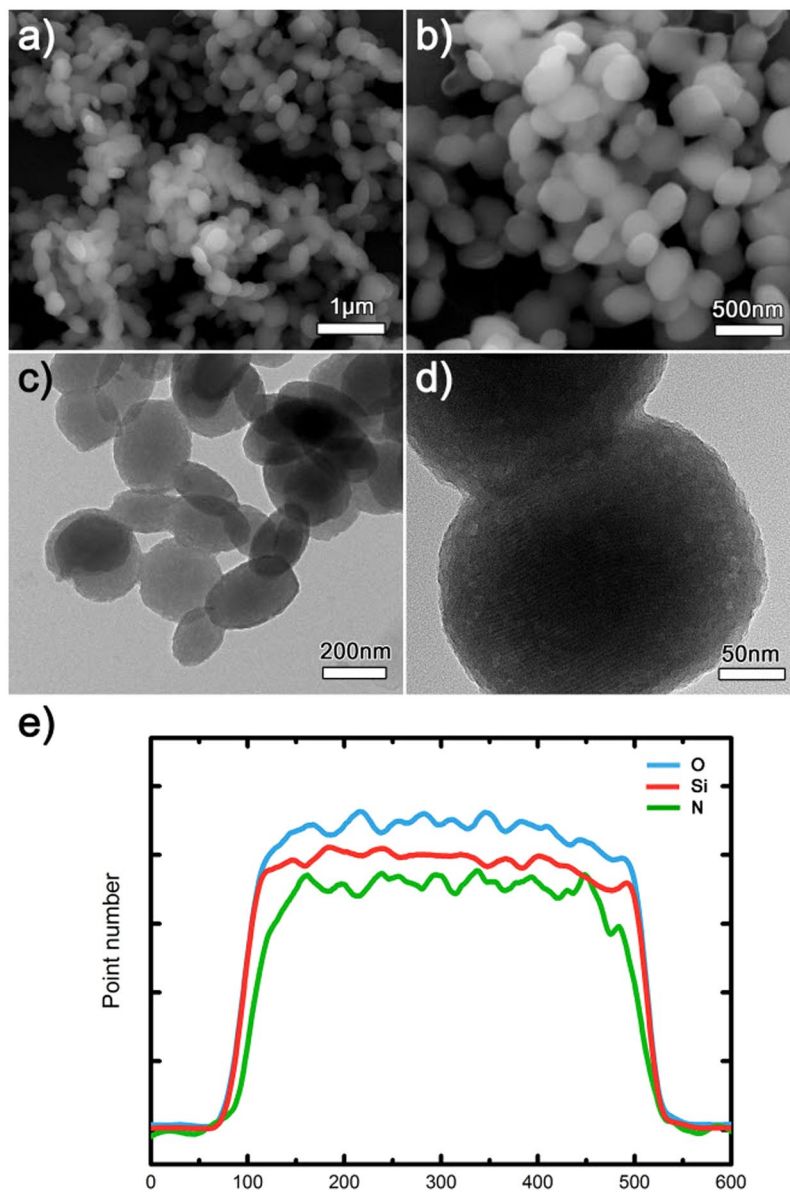


Figure 1. Morphological analyses of the PEI-silica nanoparticles with (a,b) SEM and (c,d) TEM. (e) Line scanning result (rescaled for comparison) of a nanoparticle in (d).

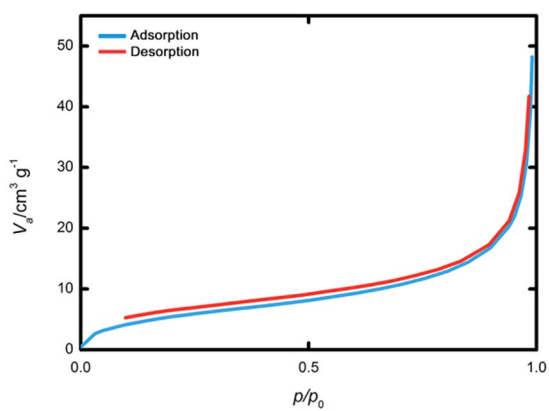


Figure 2. N_2 adsorption-desorption isotherm graph of silica nanoparticles at 77 K.

| | BET surface area [m ² /g] | Mesopore volume [cm ³ /g] |
|----------------------|---|---|
| Silica nanoparticles | 21.60 | 0.07 |

Table 1. Physical characteristic of the PEI-silica nanoparticles from the N₂ adsorption-desorption analysis.

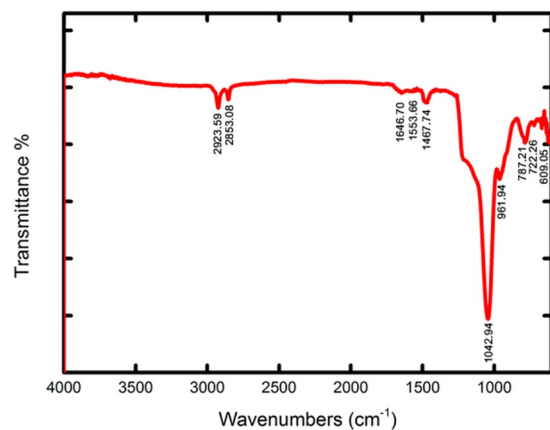


Figure 3. FT-IR spectrum of the PEI-silica nanoparticles.

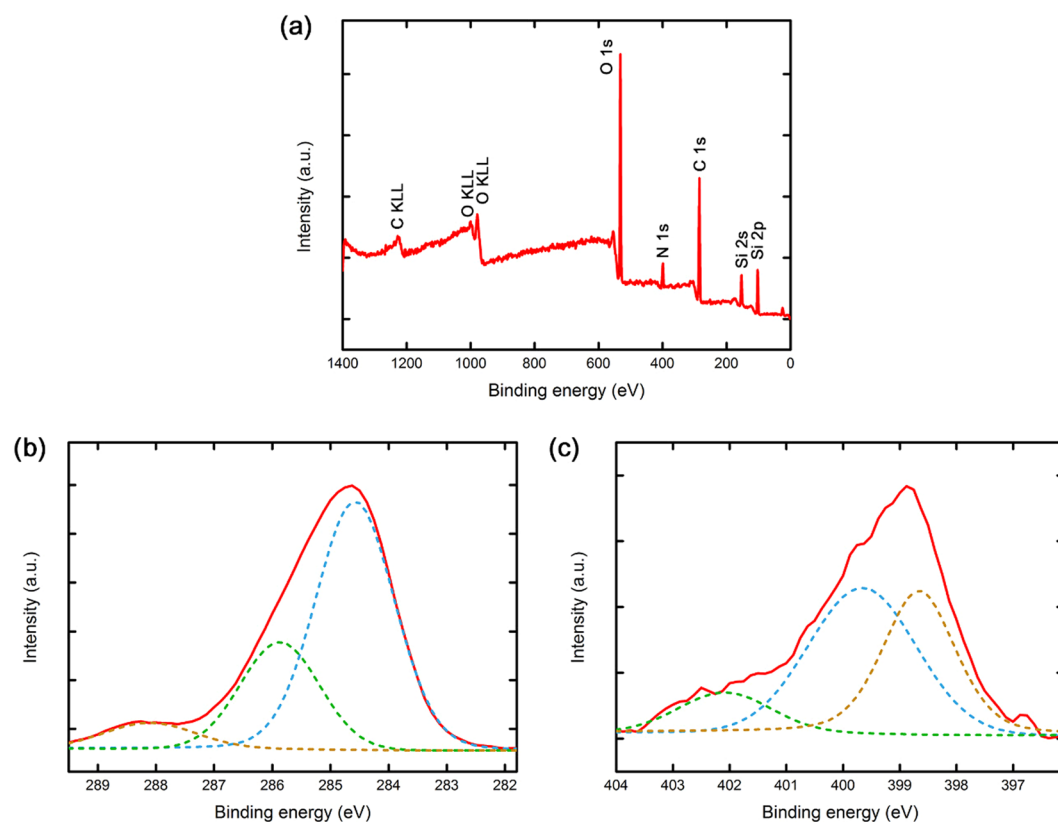


Figure 4. (a) XPS spectra of the PEI-silica nanoparticles and (b) curve-fitting for C 1s and (c) N 1s.

activated carbon (13.9 mg/g), algal bloom residue-derived activated carbon (155.52 mg/g), and metal organic frameworks (48 mg/g)^{52–56}.

Reduction of Cr(VI) Ion by N-containing PEI-silica Nanoparticle. The effect of pH on the adsorption of Cr in the solution was investigated by conducting the batch adsorption test at different initial pH levels while maintaining the other conditions as constant. The PEI-silica nanoparticles give the highest adsorption capacity

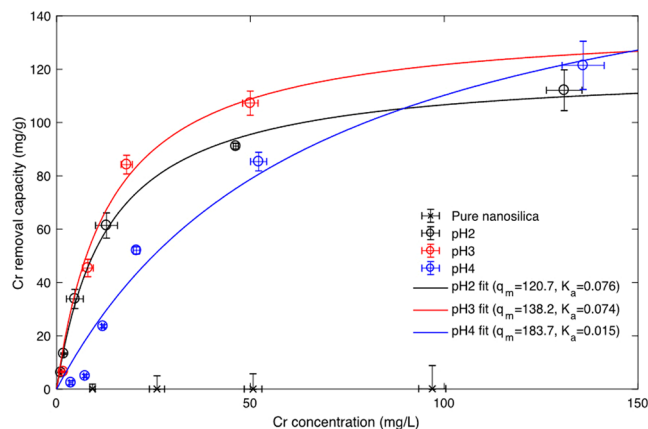


Figure 5. Cr adsorption isotherm of pure nanosilica and PEI-silica nanoparticle under pH 2, 3 and 4 and its fitting with the Langmuir adsorption model.

of 183.7 mg/g at a pH of 4 and decreases monotonically at lower and higher pH values. To identify the adsorption site and the species of the adsorbed Cr ions, we analyzed each component in PEI samples in the range of pH 2 to 4 using XPS. Figure 6 shows N XPS 1s spectra (a-c) and Cr 2p XPS spectra (d-f) of PEI samples after Cr adsorption. In the Cr 2p_{2/3} XPS spectra, three peaks are shown at approximately 575.0, 576.5, and 578.0 eV, which are assigned to Cr, CrOH, and Cr(VI), after Cr adsorption. The presence of Cr(III) ions indicates that the Cr(VI) ion is reduced in water by a N-containing functional group. Considering that the amount of trivalent chromium decreases as the pH value increases, the $-NH$ functional group can be thought to participate in the reduction reaction of Cr(VI), since the amount of the $-NH$ functional group shows the opposite trend to that of Cr(III) depending on the pH value. This reaction resembles Jones oxidation, which indicates the reduction and oxidation reactions between hydroxyl group and Cr ion, except for the $-NH$ group.

The ratio between Cr and CrOH also depends on the pH value, and the amount of Cr decreased with the pH value, while that of CrOH increased. According to the Pourbaix diagram, Cr^{3+} and $CrOH^{2+}$ are dominant in the low and high pH values in the range of pH 2 and 4, respectively³⁷. Both species of Cr(III) ions are adsorbed on PEI by making covalent bonds with N atoms, directly. On the other hand, Cr(VI) ions are adsorbed on the NH_3^+ functional group through hydrogen bonding. These adsorption behaviors will be discussed in terms of theoretical calculations in the next session. The amount of Cr(VI) ions increased with the pH value, while that of Cr(III) decreased, as mentioned above. This result indicates that the reduction reaction of Cr(VI) depends on pH value.

First Principles Calculations. We carried out first principles calculations to identify the adsorption mechanisms between Cr ions and adsorption sites in the PEI-silica nanoparticles. We investigated combinatorial configurations of three adsorbates (Cr, CrOH, and $HCrO_4^-$) and four adsorption sites ($-N=$, $-NH-$, $-NH_2$, $-NH_3$) based on the XPS spectra. The calculation results show that Cr(III) and Cr(VI) ions favor different adsorption processes. Both $Cr(OH)^{2+}$ and Cr^{3+} ions bind to N atoms directly by forming covalent bonds, of which the bond lengths between Cr and N atoms are 1.88 Å and 1.90 Å, as shown in Fig. 7(a,b), respectively. In Fig. 7(c), the density of states (DOS) for the Cr-N configuration is given and the orbital hybridization of the two atoms is given in the energy range of -2.75 eV and -2.00 eV with respect to the Fermi energy, which corresponds to the region painted in translucent yellow. We further calculated the charge density over that energy range and the shape of the partial charge density plot indicates the orbital hybridization of the d-orbital of Cr and the p-orbital of N in Fig. 7(d). On the other hand, Cr(VI) binds to $-NH_3^+$ through hydrogen bonding, as shown in Fig. 7(d). The bond lengths between three O atoms in Cr(VI) and three H atoms in $-NH_3$ are 1.55 Å, 2.00 Å, and 2.58 Å, respectively.

Conclusions

This research aimed to develop a novel nanoparticle for the removal of chromium from solution. Equilibrium batch tests were conducted to examine the adsorption capacity of the developed adsorbent. The maximum adsorption capacity for chromium was found to be 183.7 mg/g. Experiments with various initial pH values (2 to 4) were conducted under controlled conditions and found that the removal efficiency of the PEI-silica nanoparticles was affected by the solution pH, and the highest removal efficiency of chromium occurred at a pH of 4. The amine group participates in the reduction reaction of Cr(VI) to Cr(III) by oxidizing itself. The reduced Cr(III) ions, Cr^{3+} and $CrOH^{2+}$, are adsorbed on oxidized N by covalent bonding. On the other hand, Cr(VI), $HCrO_4^-$, is adsorbed on a protonated primary amine, NH_3^+ , by hydrogen bonding. These results should help improve the understanding of the chromium adsorption mechanisms from industrial wastewater in other forms of nanoparticles containing amine groups.

Materials and Methods

Materials. All chemicals were obtained from the indicated suppliers and used without further purification. Tetraethyl orthosilicate (TEOS, 99.999% metal basis), hexadecyltrimethylammonium bromide (CTAB H5882, >98%) and branched polyethyleneimine (PEI, $M_w = 800$) were purchased from Sigma-Aldrich. Cr(VI) solutions

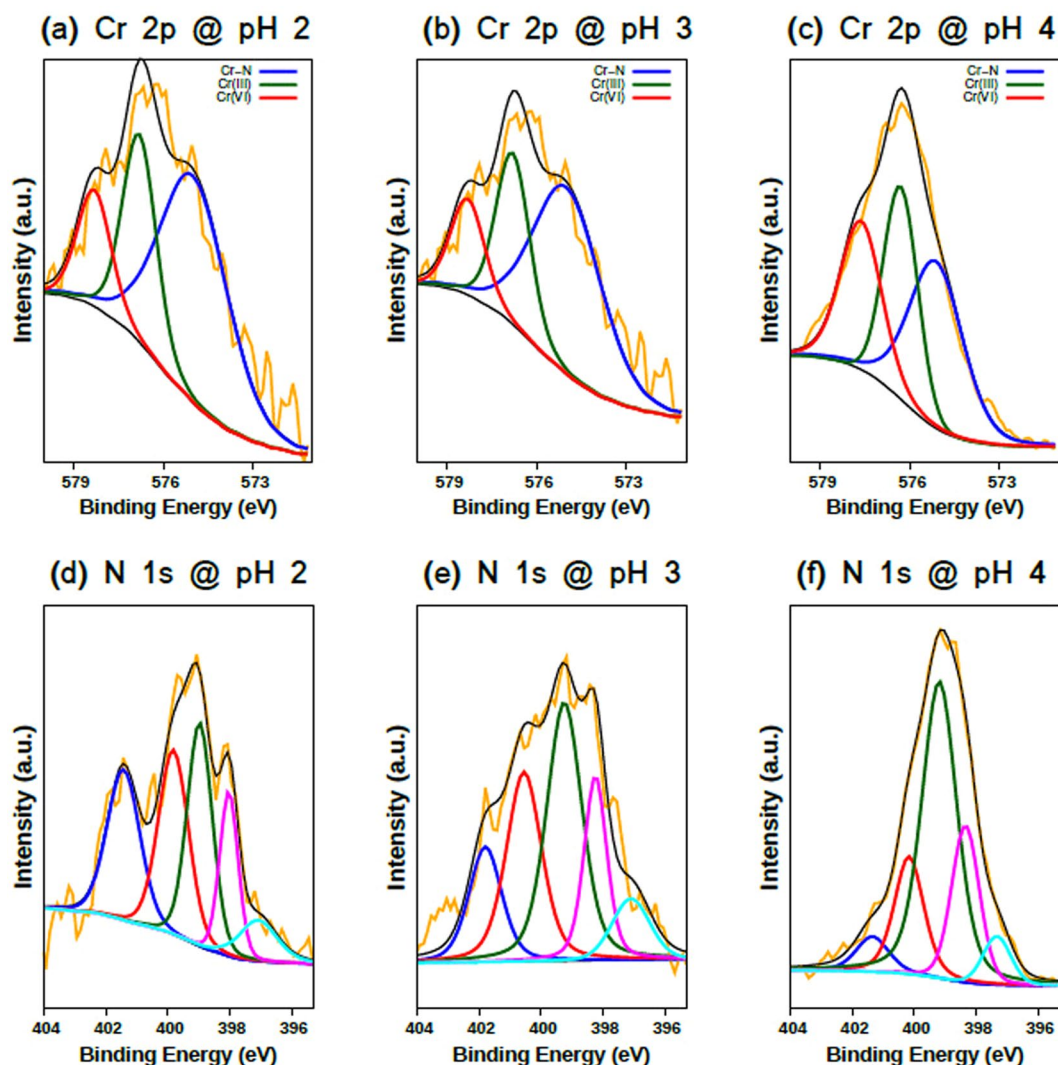


Figure 6. (a)–(c) Cr 2p XPS spectra and (d)–(h) N 1s XPS spectra of the PEI-silica nanoparticle at pH 2–4 after Cr adsorption.

were prepared by diluting Cr standard solution (Kanto Chemical, Tokyo, Japan) with deionized water. In addition, all vials and tools were cleaned with ethanol three times and deionized water three times before they were used.

Synthesis of the PEI-silica Nanoparticle. PEI-silica nanoparticles were synthesized by a one-pot technique. First, 0.656 g of CTAB were dissolved in 180 mL of distilled water and 8.5 mL of PEI were dissolved in 20 mL of ethanol as a shape and pore former. The PEI solution was mixed with the CTAB solution with stirring at 800 rpm for 30 min. Afterward, 4.2 mL of TEOS, as the silica precursor, were added using a micropipette. The solution was stirred for 12 hrs, before all final products were washed by centrifugation with distilled water three times. Finally, after drying at 70 °C overnight, we obtained 200–300 nm nanoparticles. To calculate the content of PEI in PEI-silica nanoparticles, they were calcined at 480 °C in air after 2 hr drying at 100 °C. The weight change after calcination was measured.

Synthesis of the Pure Nanosilica. For a control experiment, pure nanosilica was prepared by calcination of the PEI-silica nanoparticles. To remove the PEI polymer, they were calcined at 480 °C in air for 12 hrs.

Characterization of PEI-silica Nanoparticles. The particle sizes and morphologies were observed by scanning electron microscopy (SEM, FEI Inspect F50, AP-tech Company) and transmission electron microscopy (TEM, Tecnai G2 F20, FEI Company). FT-IR spectra were obtained by employing a Nicolet iS 10 FT-IR Spectrometer (Thermo Scientific) over the range of 4000–600 cm^{-1} . N_2 adsorption-desorption analysis was performed using a surface area analyzer (BEL-SORP-max, BEL Japan Inc., Japan). Prior to analysis, the materials were degassed at 100 °C for 2 h to obtain pure PEI-silica materials. The specific surface area was determined from the linear part of the Brunauer-Emmett-Teller (BET) plot ($P/P_0 = 0-1$). The total pore volume was evaluated from the adsorbed amount at a relative pressure of ~ 0.99 . Elements in the PEI-silica nanoparticles were analyzed by X-ray photoelectron spectroscopy (XPS) on a PHI 5000 VersaProbe Ulvac-PHI (Physical Electronics, Inc.) with

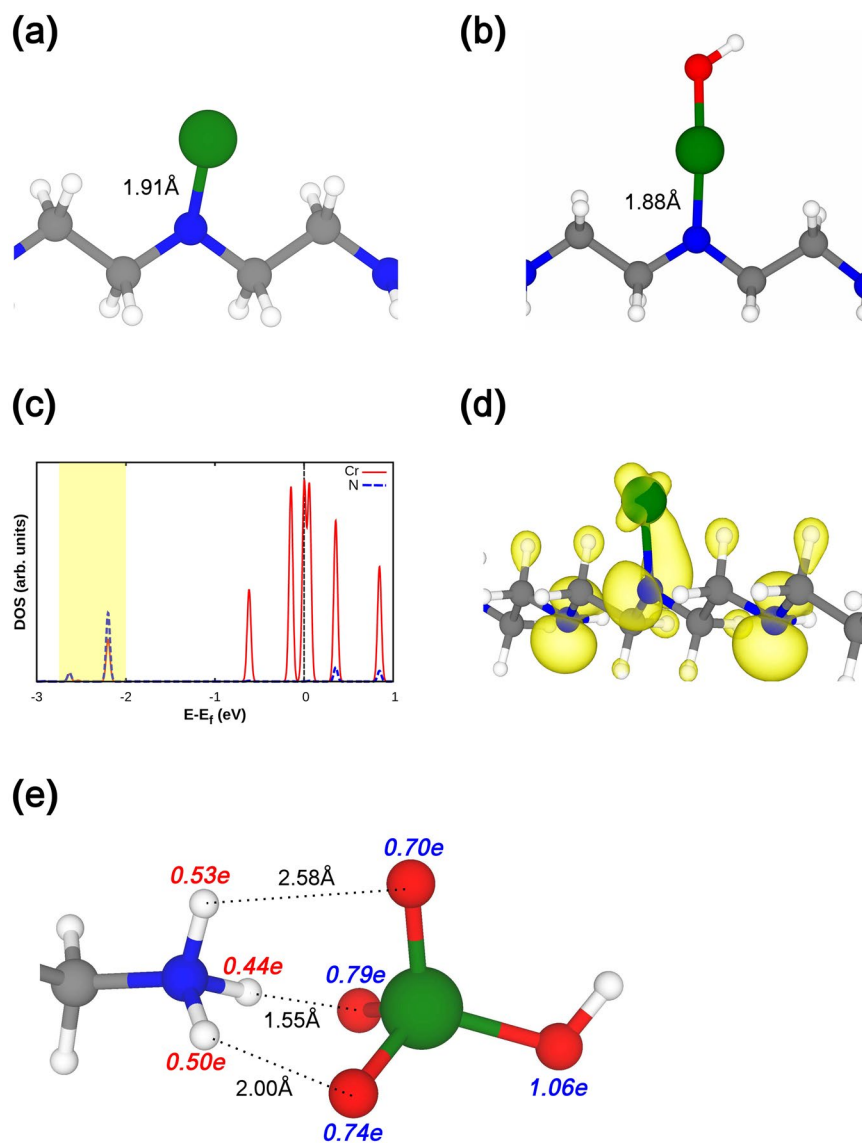


Figure 7. Cr(III), (a) Cr^{3+} and (b) $[\text{Cr}(\text{OH})_2]^{2+}$, makes a covalent bonding with oxidized secondary amine group, $-\text{N}=\text{C}$. (c) Partial density of state (PDOS) shows orbital hybridization between Cr d-orbital and N p-orbital in the energy range -2.75 to -2.00 eV (yellow shaded region). (d) The partial charge density in the same energy range also shows the orbital hybridization between Cr d-orbital and N p-orbital. The isosurface level of partial charge density is $0.1e/\text{\AA}^3$. (e) Cr(VI), $[\text{HCrO}_4]^-$, is adsorbed on protonated primary amine, NH_3^+ , by hydrogen bonding. The amount of positive (negative) charges on each atom is indicated by red (blue) number. White, grey, blue, red, and green balls represent hydrogen, carbon, nitrogen, oxygen, and chromium atom, respectively.

an Al X-ray monochromatic source of K_α (1486.6 eV energy at 24.5 W). The binding energy was referenced to the C 1s line at 284.6 eV from adventitious carbon.

Batch Experiments for Chromium Removal. Removal of chromium was subjected to equilibrium batch tests. The chromium adsorption test was conducted in 50 mL a conical tube containing 0.02~0.03 g of PEI-silica nanoparticles by adding 50 mL of chromium solutions with concentrations of 10, 20, 50, 100 and 200 mg/L. To investigate the effect of the solution pH on chromium removal, the batch experiments were conducted at the different pH levels (pH 2, 3 and 4). The desired concentrations of Cr were prepared by diluting the standard solution with deionized water. The solution pH was adjusted by adding hydrochloric acid (HCl) or sodium hydroxide (NaOH). The samples were mixed using a rotary shaker at 100 rpm for 24 hr. After the reaction was completed, the liquid phase was separated from the solution using a $0.45\ \mu\text{m}$ PTFE syringe filter (Millipore, USA). The Cr concentration and pH were measured using inductively coupled plasma optical emission spectroscopy (ICP-OES, Optima 2000DV, Perkin-Elmer) and a benchtop pH meter (Orion VERSA 5 star), respectively. Subsequently, the residual PEI-silica nanoparticles, retrieved by rotary evaporation to preserve the adsorbed ions, were analyzed

by XPS. In addition, an equilibrium adsorption test of pure nanosilica prior to the synthesis of the nanoparticles using PEI was also conducted to confirm the adsorption capacity of only silica for chromate.

For quantifying the adsorption capacity of the PEI-silica nanoparticles, the equilibrium adsorption of chromium was analyzed by the Langmuir adsorption isotherm model, which is shown in Eq. (1)⁵³:

$$q = \frac{q_m K_a C}{1 + K_a C} \quad (1)$$

where q_m is the maximum mass adsorbed under saturated conditions per unit mass of adsorbent (mg/g). K_a is an empirical constant with units of the inverse of concentration C (L/mg).

Computational Methods. We performed first-principles calculations based on density functional theory using the Vienna Ab-initio Simulation Package (VASP)⁵⁸. The general gradient approximation (GGA) was adapted for exchanging the correlation functional, and the pseudopotential was parameterized under projector augmented wave (PAW) scheme by Perdew–Burke–Emzerhof (PBE)^{59–61}. The energy cut-off on a planewave basis was 500 eV, and the force criteria for structure optimization was 0.01 eV/Å. We adopted the DFT–D3 method with Becke–Johnson damping to include van der Waals interactions^{62,63}. The lattice was set to $25 \times 20 \times 15$ Å to avoid inter-cell interactions. We analyzed the amount of charges on each atom by using bader charge analysis⁶⁴. All configurations obtained from the theoretical calculations were drawn by using VESTA⁶⁵.

Data availability. All data generated or analyzed during this study are included in this published article.

References

- Chen, X. *et al.* Recovery of valuable metals from waste cathode materials of spent lithium-ion batteries using mild phosphoric acid. *J. Hazard. Mater.* **326**, 77–86 (2017).
- Rebelo, F. M. & Caldas, E. D. Arsenic, lead, mercury and cadmium: Toxicity, levels in breast milk and the risks for breastfed infants. *Environ. Res.* **151**, 671–88 (2016).
- Liu, D. *et al.* Heavy metal pollution in urban soil from 1994 to 2012 in Kaifeng City, China. *Water Air Soil Pollut.* **227**, 154 (2016).
- Shahid, M. *et al.* Foliar heavy metal uptake, toxicity and detoxification in plants: A comparison of foliar and root metal uptake. *J. Hazard. Mater.* **325**, 36–58 (2017).
- Kumar, G. H. & Kumari, J. P. Heavy metal lead influent toxicity and its assessment in phytoremediating plants—A review. *Water Air Soil Pollut.* **226**, 324 (2015).
- Crisostomo, C. A. B. *et al.* Joint assessment of bioreduction of chromium(VI) and of removals of both total chromium and total organic carbon (TOC) in sequential hybrid bioreactors. *Water Air Soil Pollut.* **227**, 51 (2016).
- Zhou, J. *et al.* Effective removal of hexavalent chromium from aqueous solutions by adsorption on mesoporous carbon microspheres. *J. Colloid Interf. Sci.* **462**, 200–7 (2016).
- Cheng, Q. *et al.* Hexavalent chromium removal using metal oxide photocatalysts. *Appl. Catal. B* **176–177**, 740–8 (2015).
- Li, L. L. *et al.* Cr(VI) removal via anion exchange on a silver-triazolate MOF. *J. Hazard. Mater.* **321**(5), 622–8 (2017).
- Song, B. *et al.* Evaluation methods for assessing effectiveness of *in situ* remediation of soil and sediment contaminated with organic pollutants and heavy metals. *Environ. Int.* **105**, 43–55 (2017).
- Riaz, T. *et al.* Synthesis and characterization of polyurethane-cellulose acetate blend membrane for chromium(VI) removal. *Carbohydr. Polym.* **153**, 582–91 (2016).
- Sadyrbaeva, T. Z. Removal of chromium(VI) from aqueous solutions using a novel hybrid liquid membrane-electrodialysis process. *Chem. Eng. Process.* **99**, 183–91 (2016).
- Golbaz, S. *et al.* Separate and simultaneous removal of phenol, chromium, and cyanide from aqueous solution by coagulation/precipitation: Mechanisms and theory. *Chem. Eng. J.* **253**, 251–7 (2014).
- Mishra, A., Tripathi, B. D. & Rai, A. K. Packed-bed column biosorption of chromium(VI) and nickel(II) onto *Fenton* modified *Hydrilla verticillata* dried biomass. *Ecotox. Environ. Safe.* **132**, 420–8 (2016).
- Lu, M. *et al.* Preparation of TiO₂/silicate-2@CoFe₂O₄ magnetic composites and evaluation of their photocatalytic activity in Cr(VI) removal. *Water Air Soil Pollut.* **225**, 295 (2015).
- Liu, W., Ni, J. & Yin, X. Synergy of photocatalysis and adsorption for simultaneous removal of Cr(VI) and Cr(III) with TiO₂ and titanate nanotubes. *Water Res.* **53**, 12–25 (2014).
- Song, B. *et al.* Effect of multi-walled carbon nanotubes on phytotoxicity of sediments contaminated by phenanthrene and cadmium. *Chemosphere* **172**, 449–58 (2017).
- Xiao, Z. *et al.* Ultra-efficient removal of chromium from aqueous medium by biogenic iron based nanoparticles. *Sep. Purif. Technol.* **174**, 466–73 (2017).
- Ma, H. *et al.* Adsorptive removal of trivalent chromium in aqueous solution using precipitate produced from aluminum tanning wastewater. *Water Air Soil Pollut.* **225**, 1956 (2014).
- Wu, Z. X. & Zhao, D. Y. Ordered mesoporous materials as adsorbents. *Chem. Commun.* **47**, 3332–8 (2011).
- Mohan, D., Singh, K. P. & Singh, V. K. Removal of hexavalent chromium from aqueous solution using low-cost activated carbons derived from agricultural waste materials and activated carbon fabric cloth. *Ind. Eng. Chem.* **44**, 1027–42 (2005).
- Ko, K. R., Ryu, S. K. & Park, S. J. Effect of ozone treatment on Cr(VI) and Cu(II) adsorption behaviors of activated carbon fibers. *Carbon* **42**, 1864–7 (2004).
- Yusof, A. M. & Malek, N. A. N. N. Removal of Cr(VI) and As(V) from aqueous solution by HDTMA-modified zeolite Y. *J. Hazard. Mater.* **162**, 1019–24 (2009).
- Ghiaci, M. *et al.* Adsorption of chromate by surfactant-modified zeolites and MCM-41 molecular sieve. *Sep. Purif. Technol.* **40**, 285–95 (2004).
- Li, Z. & Bowman, R. S. Counterion effects on the sorption of cationic surfactant and chromate on natural clinoptilolite. *Environ. Sci. Technol.* **31**, 2407–12 (1997).
- Krishna, B. S., Murty, D. S. R. & Jai Prakash, B. S. Surfactant-modified clay as adsorbent for chromate. *Appl. Clay Sci.* **20**, 65–71 (2001).
- Khan, S. A. Riaz ur, R. & Khan, M. A. Adsorption of chromium (III), chromium (VI) and silver (I) on bentonite. *Waste Manage.* **15**, 271–82 (1995).
- Dinker, M. K. & Kulkarni, P. S. Recent advances in silica-based materials for the removal of hexavalent chromium: a review. *J. Chem. Eng. Data* **60**, 2521–40 (2015).
- Wight, A. P. & Davis, M. E. Design and preparation of organic-inorganic hybrid catalysts. *Chem. Rev.* **102**, 2589–3614 (2002).
- Yoshitake, H., Yokoi, T. & Tatsumi, T. Adsorption of chromate and arsenate by amino-functionalized MCM-41 and SBA-1. *Chem. Mater.* **14**, 4603–10 (2002).

31. Li, J. *et al.* Different N-containing functional groups modified mesoporous adsorbents for Cr(VI) sequestration: Synthesis, characterization and comparison. *Micropor. Mesopor. Mat.* **110**, 442–50 (2008).
32. Lam, K. F., Yeung, K. L. & McKay, G. Selective mesoporous adsorbents for and Cu²⁺ separation. *Micropor. Mesopor. Mat.* **100**, 191–201 (2007).
33. Hideaki, Y., Toshiyuki, Y. & Takashi, T. Oxyanion adsorptions by mono-, di-, and triamino-functionalized MCM-48. *B. Chem. Soc. Jpn.* **76**, 847–52 (2003).
34. Anbia, M., Mohammadi, N. & Mohammadi, K. Fast and efficient mesoporous adsorbents for the separation of toxic compounds from aqueous media. *J. Hazard. Mater.* **176**, 965–72 (2010).
35. Park, H. J. & Tavlarides, L. L. Adsorption of chromium (VI) from aqueous solutions using an imidazole functionalized adsorbent. *Ind. Eng. Chem. Res.* **47**, 3401–9 (2008).
36. Zaitseva, N., Zaitsev, V. & Walcarius, A. Chromium (VI) removal via reduction-sorption on bi-functional silica adsorbents. *J. Hazard. Mater.* **250–51**, 454–61 (2013).
37. Perez-Quintanilla, D. *et al.* Cr(VI) adsorption on functionalized amorphous and mesoporous silica from aqueous and non-aqueous media. *Mater. Res. Bull.* **42**, 1518–30 (2007).
38. Arkas, M. & Tsiourvas, D. Organic/inorganic hybrid nanospheres based on hyperbranched poly(ethylene imine) encapsulated into silica for the sorption of toxic metal ions and polycyclic aromatic hydrocarbons from water. *J. Hazard. Mater.* **170**, 35–42 (2009).
39. Cao, N. *et al.* Fabrication of SnO₂/porous silica/polyethyleneimine nanoparticles for pH-responsive drug delivery. *Mat. Sci. Eng. C-Mater.* **59**, 319–23 (2016).
40. Lippincott, E. *et al.* Infrared studies on polymorphs of silicon dioxide and germanium dioxide. *J. Res. Natl. Ins. Stand. Technol.* **61**, 61–70 (1958).
41. Rekha, P., Sharma, V. & Mohanty, P. Synthesis of cyclophosphazene bridged mesoporous organosilicas for CO₂ capture and Cr(VI) removal. *Micropor. Mesopor. Mat.* **219**, 93–102 (2016).
42. Choi, S. W. & Bae, H. K. Adsorption of CO₂ on amine-impregnated mesoporous MCM-41 silica. *Ksce. J. Civ. Eng.* **18**, 1977–83 (2014).
43. Li, Y. *et al.* Synthesis of amine-modified mesoporous materials for CO₂ capture by a one-pot template-free method. *J. Sol-Gel Sci. Technol.* **66**, 353–62 (2013).
44. Wang, K. *et al.* Efficient CO₂ capture on low-cost silica gel modified by polyethyleneimine. *J. Nat. Gas Chem.* **21**, 319–23 (2012).
45. Klunkowski, A. M. *et al.* Coordination state of copper(II) complexes anchored and grafted onto the surface of organically modified silicates. *Langmuir* **15**, 5814–19 (1999).
46. Shimizu, I. *et al.* Diffuse reflectance infrared Fourier transform spectral study of the thermal and adsorbed-water effects of a 3-aminopropyltriethoxysilane layer modified onto the surface of silica gel. *Vib. Spectrosc.* **14**, 113–23 (1997).
47. Yu, J. G., Le, Y. & Cheng, B. Fabrication and CO₂ adsorption performance of bimodal porous silica hollow spheres with amine-modified surfaces. *Rsc. Adv.* **2**, 6784–91 (2012).
48. Wang, X. L. *et al.* Impact of polyethyleneimine conjugation mode on the cell transfection efficiency of silica nanovectors. *Langmuir* **31**, 11078–85 (2015).
49. Khader, M. M. *et al.* Adsorption of CO₂ on polyethyleneimine 10k-Mesoporous silica sorbent: XPS and TGA studies. *Am. J. Anal. Chem.* **6**, 274–84 (2015).
50. Islam, M. S., Choi, S. W. & Lee, H. J. Controlled etching of internal and external structures of SiO₂ nanoparticles using hydrogen bond of polyelectrolytes. *ACS Appl. Mater. Inter.* **6**, 9563–71 (2014).
51. Drese, J. *et al.* Synthesis-structure-property relationships for hyperbranched aminosilica CO₂ adsorbents. *Adv. Funct. Mater.* **19**, 3821–32 (2009).
52. Choi, J. W. *et al.* Surface modified mesostructured iron oxyhydroxide: synthesis, ecotoxicity, and application. *Water Environ. Res.* **86**(12), 2338–46 (2014).
53. Ko, Y. J. *et al.* Chromate adsorption mechanism on nanodiamond-derived onion-like carbon. *J. Hazard. Mater.* **320**, 368–75 (2016).
54. Liu, S. X. *et al.* Activated carbon with excellent chromium(VI) adsorption performance prepared by acid-base surface modification. *J. Hazard. Mater.* **141**, 315–9 (2007).
55. Yue, Z. R. *et al.* Removal of chromium Cr(VI) by low-cost chemically activated carbon materials from water. *J. Hazard. Mater.* **166**, 74–8 (2009).
56. Maleki, A. *et al.* Adsorption of hexavalent chromium by metal organic frameworks from aqueous solution. *J. Ind. Eng. Chem.* **28**, 211–6 (2015).
57. Beverskog, B. & Puigdomenech, I. Revised Pourbaix diagrams for chromium at 25–300 degrees C. *Corros Sci.* **39**, 43–57 (1997).
58. Kresse, G. & Furthmüller, J. Efficiency of ab-initio total energy calculations for metals and semiconductors using a plane-wave basis set. *Comput. Mater. Sci.* **6**, 15–50 (1996).
59. Perdew, J. P., Burke, K. & Ernzerhof, M. Generalized gradient approximation made simple. *Phys. Rev. Lett.* **77**, 3865–8 (1996).
60. Blöchl, P. E. Projector augmented-wave method. *Phys. Rev. B* **50**, 17953–79 (1994).
61. Kresse, G. & Joubert, D. From ultrasoft pseudopotentials to the projector augmented-wave method. *Phys. Rev. B* **59**, 1758–75 (1999).
62. Grimme, S. *et al.* A consistent and accurate ab initio parametrization of density functional dispersion correction (DFT-D) for the 94 elements H-Pu. *J. Chem. Phys.* **132**, 154104 (2010).
63. Grimme, S., Ehrlich, S. & Goerigk, L. Effect of the damping function in dispersion corrected density functional theory. *J. Comput. Chem.* **32**, 1456–65 (2011).
64. Yu, M. & Trinkle, D. R. Accurate and efficient algorithm for Bader charge integration. *J. Chem. Phys.* **134**, 064111 (2011).
65. Momma, K. & Izumi, F. VESTA: a three-dimensional visualization system for electronic and structural analysis. *J. Appl. Cryst.* **41**, 653–8 (2008).

Acknowledgements

This research was supported by the Korea Institute of Science and Technology (KIST) institutional program (Grant No. 2E28120) and the Korea Ministry of Environment (MOE) as “Public Technology Program based on Environmental Policy (E416-00020-0606-0)”. J.H.L. at UNIST was supported by the Basic Science Research Program through the National Research Foundation of Korea (NRF) funded by the Ministry of Science, ICT & Future Planning (2015R1C1A1A01055760). This study was also partly supported by a Korea CCS R&D Center (Korea CCS 2020 Project) grant funded by the Korean Government (Ministry of Science, ICT & Future Planning) in 2017 (KCRC-2014M1A8A1049315).

Author Contributions

J.O.P and J.-A.P performed all experiments. S.L., S.Y.L., S.-H.C. and J.-W.C. wrote the main manuscript text and J.-A. prepared all figures. K.C. and J.L. performed first-principles calculations. All authors reviewed the whole manuscript.

Additional Information

Supplementary information accompanies this paper at <https://doi.org/10.1038/s41598-018-20017-9>.

Competing Interests: The authors declare that they have no competing interests.

Publisher's note: Springer Nature remains neutral with regard to jurisdictional claims in published maps and institutional affiliations.



Open Access This article is licensed under a Creative Commons Attribution 4.0 International License, which permits use, sharing, adaptation, distribution and reproduction in any medium or format, as long as you give appropriate credit to the original author(s) and the source, provide a link to the Creative Commons license, and indicate if changes were made. The images or other third party material in this article are included in the article's Creative Commons license, unless indicated otherwise in a credit line to the material. If material is not included in the article's Creative Commons license and your intended use is not permitted by statutory regulation or exceeds the permitted use, you will need to obtain permission directly from the copyright holder. To view a copy of this license, visit <http://creativecommons.org/licenses/by/4.0/>.

© The Author(s) 2018